Polarization-based surface normal estimation of black specular objects from multiple viewpoints

Daisuke Miyazaki, Takuya Shigetomi, Masashi Baba, Ryo Furukawa, Shinsaku Hiura, and Naoki Asada
Graduate School of Information Sciences
Hiroshima City University
Hiroshima, JAPAN
Website: http://ime.info.hiroshima-cu.ac.jp/

Abstract—**Polarization is physical phenomena of the light which gives rich information of the scene even though it is undetectable by human eyes. In this paper, we analyze the polarization state of the light reflected on black specular objects in order to estimate the surface normal of the objects. Since polarization image of single view is not enough to uniquely determine the surface normal, we observe the object from multiple views. A rough estimate of the object geometry is obtained a priori by space carving so that the polarization state of the reflected light can be analyzed at the same surface point under multiple views. Unlike the photometric stereo or the multiview stereo which cannot estimate the surface normal and the geometry of black specular objects, the proposed method which is based on the polarization analysis and the space carving can estimate the surface normal and the geometry of black specular objects.**

Keywords-**polarization; shape-from-X; surface normal; space carving; specular reflection;**

I. INTRODUCTION

3D modeling techniques have wide applications, including cinema, computer games, digital content on the Internet, virtual space, and digital archiving. The purpose of digital archiving is to digitize, preserve, and exhibit the cultural materials stored in museums. Therefore, 3D modeling has one of the most important roles in digital archiving. One approach for creation of a 3D model is to use a laser range sensor. However, laser range sensors are expensive and take a long time to obtain the data. Therefore, alternative methods to estimate the shapes quickly, easily, and precisely are desired. 3D modeling techniques are also heavily investigated in the field of computer vision. The techniques used can be categorized into two types. One is the geometric approach, which uses the geometrical structure of the scene, and the other is the photometric approach, which uses the light reflected from the scene.

Space carving [9], [12] is a geometric approach which estimates the 3D coordinates from multiple viewpoints. Unlike multi-view stereo, the space carving method can estimate the shape of a textureless black object even if it has high specularity. However, the problem with space carving is that a smooth surface cannot be obtained.

However, a smooth surface normal can be obtained by a photometric approach. Polarization [4], [6], [23] is one of the quantities that can be used to obtain a smooth surface normal. Koshikawa and Shirai [8] used circular polarization to estimate the surface normal of a specular object. Saito *et al.* [22] proposed the basic theory to estimate the surface normal of a transparent object using polarization. Miyazaki *et al.* [13] estimated the surface normal of a transparent object by analyzing the polarization state of the thermal radiation from the object. Miyazaki *et al.* [14] also tried to estimate the surface normal of a diffuse object from a single view. Miyazaki *et al.* [15] also used a geometrical invariant to match the corresponding points from two views to estimate the surface normal of a transparent object. Miyazaki and Ikeuchi [16] solved the inverse problem of polarization ray tracing to estimate the surface normal of a transparent object. Wolff and Boult [25] developed the basic theory to show that polarization analysis can estimate a surface normal from two views if the corresponding points are known. Rahmann [19] indicated that the surface normal can be obtained from the polarization. Rahmann and Canterakis [20] estimated the surface normal of a specular object from multiple views by iteratively finding the corresponding points of these views. Rahmann [21] proved that polarization analysis can only estimate quadratic surfaces if the corresponding points are searched iteratively. Atkinson and Hancock [1] integrated the surface normal of the local area up to a partial shape to match the shapes from two viewpoints so that they could calculate the surface normal using the polarization. Atkinson and Hancock [3] also used the partially integrated shape of a partial region and a geometrical invariant to find the corresponding points of two views so that they could calculate the surface normal using the polarization. Atkinson and Hancock [2] also provided a detailed investigation for estimation of the surface normal of a diffuse object from a single view. These methods are useful for estimating the surface normal of a specular object; however, the corresponding points of multiple views are required for the estimation process.

Recently, some researchers have integrated the geometric approach with the photometric approach to obtain rich

information about the object shape. They combine the rough 3D geometry obtained using multi-view stereo or laser range sensors with the smooth surface normal obtained using the photometric stereo method [26]. Ochiai *et al.* [17] mapped the surface normal obtained from photometric stereo measurements on to the mesh model obtained from a 3D laser sensor. Fua and Leclerc [5] combined binocular stereo and shading information, and obtained the shape of an object represented by facets. Maki *et al.* [11], Zhang *et al.* [27], Lim *et al.* [10], and Higo *et al.* [7] observed an object using a single light source and a single camera, and obtained the 3D shape of a textureless diffuse object. Zickler *et al.* [28] proposed a so-called Helmholtz stereo method, which can estimate the 3D geometry and surface normal of an object which has an arbitrary bidirectional reflectance distribution function (BRDF). These methods imply that the combination of the geometric approach and the photometric approach is quite important; however, these photometric stereo methods can only obtain the surface normal of a diffuse surface, except for the Helmholtz stereo method. The dense surface normal of a specular black object cannot be obtained by the Helmholtz stereo method because of the discretized sampling of the light source.

In this paper, we propose a method to create a 3D model using both polarization analysis and space carving. The main target objects are smooth surfaces, such as plastics and ceramics. We first calibrate the multiple cameras to calculate the geometrical relationships between the multiple cameras. We observe the object from multiple viewpoints with a polarization imaging camera. First, we apply space carving to estimate the rough structure of the object. Space carving can obtain a visual hull of a textureless object; however, it cannot obtain the shape of a concave part of the object. The 3D shape obtained by conventional space carving is usually not smooth; thus, we add the polarization information. The shape-from-polarization method can estimate the shapes of highly specular objects, such as black objects, which cannot be estimated by the photometric stereo method. The polarization information of the object is obtained from multiple viewpoints by a polarization imaging camera. The polarization data should be analyzed at identical points on the object surface when observed from multiple viewpoints; thus, the shape obtained by the space carving can be used for estimation of the surface normal from the polarization data. We map the surface normal obtained from the polarization information onto the 3D surface of the object.

We describe our method in Section II, and we give our results in Section III. We conclude the paper in Section IV, and also discuss the advantages and disadvantages of our method.
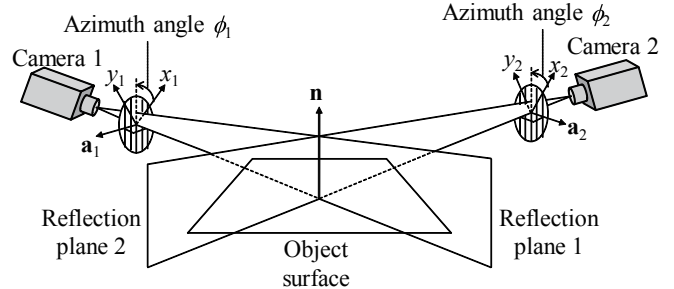

Figure 1. Relationship between the surface normal and the reflection plane when observed from two viewpoints.

II. ESTIMATING THE SURFACE NORMAL FROM POLARIZATION INFORMATION OBTAINED FROM MULTIPLE VIEWS

A. Phase angle and surface normal

We illuminate the object with unpolarized light, and observe the reflected light with the polarization imaging camera. We denote the plane that includes the incident light ray and the surface normal as the reflection plane. We assume that the surface is smooth; thus, the reflected light ray is also included in the reflection plane.

By rotating a linear polarizer set in front of the camera, the observed light changes from bright to dark. The cycle of oscillation of the brightness is $180°$, and we denote the maximum and minimum brightness values as $I_{\max}$ and $I_{\min}$, respectively. The polarizer angle when the maximum brightness $I_{\max}$ is observed is defined as the phase angle ψ. If we observe the specular reflection of the dielectric object, the polarizer angle when $I_{\min}$ is observed represents the angle of the reflection plane. We denote the azimuth angle of the surface normal $\mathbf{n} = (n_x, n_y, n_z)^\top$ as ϕ, and the zenith angle as θ. Therefore, the azimuth angle of the surface normal and the phase angle are related as $\phi = \psi + 90° \pm 180°$.

B. Calculating the surface normal from two viewpoints

Section II-A has described the relationship between the surface normal and the phase angle. However, we cannot determine the surface normal uniquely, because only the orientation of the reflection plane including the surface normal is obtained. We must observe the object from two viewpoints to solve this problem.

We analyze the two phase angles at the same surface point, corresponding to the known 3D geometry. The relationship between the surface normal vector and the azimuth angle is shown in Fig. 1, and the azimuth angle is $90°$ rotated from the phase angle. The relationship between the azimuth angles for each of the cameras, represented as ϕ_1 and ϕ_2, and the normal vector of the reflection plane represented as
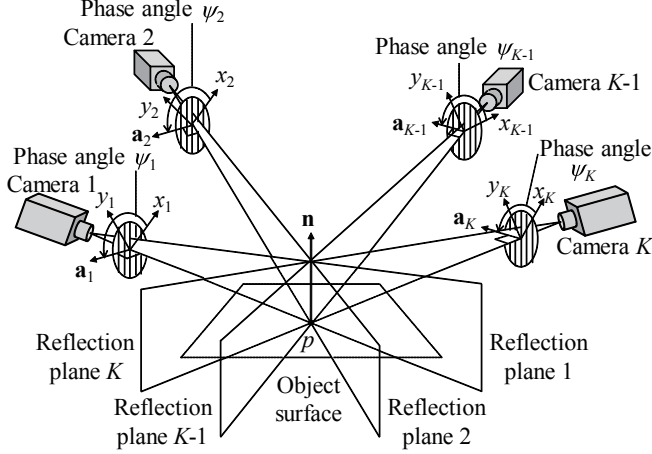
Figure 2. Relationship between the surface normal and the phase angle observed from multiple viewpoints.

$\mathbf{a}_1$ and $\mathbf{a}_2$, is shown in Eq. (1).

$$\mathbf{a}_1 = \begin{pmatrix} \cos(\phi_1 + 90°) \\ \sin(\phi_1 + 90°) \\ 0 \end{pmatrix} = \begin{pmatrix} \cos\psi_1 \\ \sin\psi_1 \\ 0 \end{pmatrix}, \quad (1)$$

$$\mathbf{a}_2 = \begin{pmatrix} \cos(\phi_2 + 90°) \\ \sin(\phi_2 + 90°) \\ 0 \end{pmatrix} = \begin{pmatrix} \cos\psi_2 \\ \sin\psi_2 \\ 0 \end{pmatrix}. \quad (2)$$

As shown in Fig. 1, the surface normal $\mathbf{n}$ is orthogonal to the vectors $\mathbf{a}_1$ and $\mathbf{a}_2$. After projecting the vectors $\mathbf{a}_1$ and $\mathbf{a}_2$ to the world coordinate system, we can calculate the surface normal $\mathbf{n}$. The rotation matrix which projects the world coordinate system to each camera coordinate system is represented as $\mathbf{R}_1$ and $\mathbf{R}_2$ in this paper. The inverse of each of these rotation matrices is their transpose, and they project back from the camera coordinate system to the world coordinate system. Since Eq. (3) and Eq. (4) hold, we derive Eq. (5).

$$(\mathbf{R}_1^\top \mathbf{a}_1) \cdot \mathbf{n} = 0, \quad (3)$$

$$(\mathbf{R}_2^\top \mathbf{a}_2) \cdot \mathbf{n} = 0, \quad (4)$$

$$\begin{pmatrix} \mathbf{a}_1^\top \mathbf{R}_1 \\ \mathbf{a}_2^\top \mathbf{R}_2 \\ \mathbf{0} \end{pmatrix} \begin{pmatrix} n_x \\ n_y \\ n_z \end{pmatrix} = \begin{pmatrix} 0 \\ 0 \\ 0 \end{pmatrix}. \quad (5)$$

C. Calculating the surface normal from multiple viewpoints

This section explains the estimation process for the surface normal from the phase angle obtained from multiple viewpoints. The fundamental theory is similar to that explained in Section II-B.

Fig. 2 shows the relationship between the surface normal $\mathbf{n}$ of the surface point p and the phase angle obtained from K viewpoints. In Fig. 2, ψ_k represents the phase angle of the surface point p observed by the camera $k = (1, 2, \cdots, K)$,

and $\mathbf{a}_k$ represents the vector orthogonal to the reflection plane under the coordinate system of the camera k. Because the $\mathbf{a}_k$ is orthogonal to the reflection plane, we obtain Eq. (6) using the phase angle ψ_k.

$$\mathbf{a}_k = \begin{pmatrix} \cos\psi_k \\ \sin\psi_k \\ 0 \end{pmatrix}. \quad (6)$$

The rotation matrix $\mathbf{R}_k$ represents the transformation from the world coordinates system to the local coordinates system of the camera indicated by k. The transformation from the local coordinates system of the camera k to the world coordinates system is the transpose of $\mathbf{R}_k$. Because the transformed vector becomes orthogonal to the surface normal $\mathbf{n} = (n_x, n_y, n_z)$, Eq. (7) holds.

$$(\mathbf{R}_k^\top \mathbf{a}_k) \cdot \mathbf{n} = 0, \quad (k = 1, 2, \cdots, K). \quad (7)$$

If we concatenate Eq. (7) for K cameras, we obtain Eq. (8).

$$\begin{pmatrix} \mathbf{a}_1^\top \mathbf{R}_1 \\ \mathbf{a}_2^\top \mathbf{R}_2 \\ \vdots \\ \mathbf{a}_K^\top \mathbf{R}_K \end{pmatrix} \begin{pmatrix} n_x \\ n_y \\ n_z \end{pmatrix} = \begin{pmatrix} 0 \\ 0 \\ \vdots \\ 0 \end{pmatrix},$$
$$\mathbf{A}\mathbf{n} = \mathbf{0}. \quad (8)$$

The surface normal $\mathbf{n}$, which satisfies Eq. (8) in a least squares sense, can be estimated using SVD (singular value decomposition). The $K{\times}3$ matrix $\mathbf{A}$ can be decomposed by SVD as follows.

$$\begin{pmatrix} \mathbf{a}_1^\top \mathbf{R}_1 \\ \mathbf{a}_2^\top \mathbf{R}_2 \\ \vdots \\ \mathbf{a}_K^\top \mathbf{R}_K \end{pmatrix} = \mathbf{UWV}^\top$$

$$= \mathbf{U} \begin{pmatrix} w_1 & & \\ & w_2 & \\ & & 0 \end{pmatrix} \begin{pmatrix} \mathbf{v}_1 \\ \mathbf{v}_2 \\ \mathbf{v}_3 \end{pmatrix} \quad (9)$$

Here, $\mathbf{U}$ is a $K{\times}3$ orthogonal matrix, $\mathbf{W}$ is the $3{\times}3$ diagonal matrix with non-negative values, and $\mathbf{V}^\top$ is a $3{\times}3$ orthogonal matrix. The diagonal item w_i of the matrix $\mathbf{W}$ is the singular value of the matrix $\mathbf{A}$, and the singular vector corresponding to w_i is $\mathbf{v}_i$. Due to the relationship between the surface normal and the reflection planes, the rank of the matrix $\mathbf{A}$ is at most 2; thus, one of the three singular values becomes 0. The surface normal $\mathbf{n}$ can be represented as Eq. (10) [18], which can be calculated from the singular vector which has the smallest singular value; namely, the third row of $\mathbf{V}^\top$ in Eq. (9).

$$\mathbf{n} = s\mathbf{v}_3^\top. \quad (10)$$

In the general case, s is an arbitrary scalar coefficient; however, since the surface normal and the singular vectors are normalized vectors, s would be either $+1$ or -1. Whether s should be positive or negative can be easily determined so
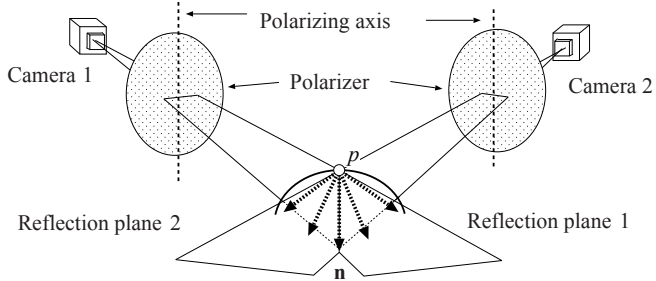
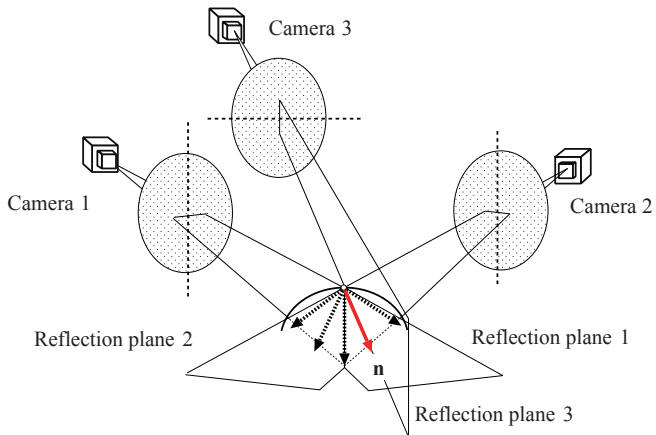Figure 3. The case where the surface normal lies on the epipolar plane of two cameras.

Figure 4. Three linearly independent cameras can estimate the surface normal of the whole surface.

that the surface normal will face towards the camera. The surface normal estimated by Eq. (10) is the optimal value which minimizes the squared error of Eq. (8) formulated by K equations. The input data should be obtained from two or more viewpoints, since the rank of the matrix $\mathbf{A}$ is two. If we obtain the input data from more viewpoints, the influence of the input noise will decrease.

If the reflection planes of the two cameras used are coplanar, as shown in Fig. 3, the surface normal cannot be uniquely determined. In this degenerated case, the rank of the matrix $\mathbf{A}$ is 1. As shown in Fig. 4, an extra camera can solve this problem. If we have three or more cameras which are not colinear, we can uniquely determine the surface normal at any point on the object surface that is observed by these cameras.

D. Algorithm flow

Fig. 5 shows the algorithm flow of the proposed method, including the input and the output for each process. In Fig. 5, the angular rectangle represents the process, and the rounded rectangle represents the input and the output.

First, we calibrate the cameras, then illuminate the object using a lighting dome, and then obtain the polarization
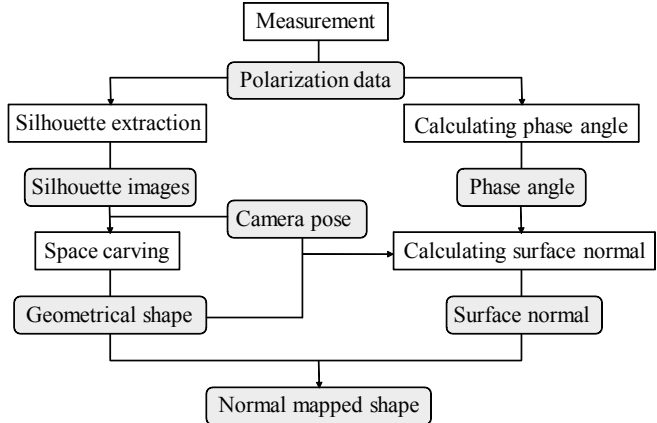

Figure 5. Algorithm flow.

images from multiple viewpoints. Next, we extract the silhouette of the target object from the image using the background subtraction method, and obtain the 3D shape of the visual hull from the camera parameters and the silhouette images by the space carving method. Finally, we calculate the phase angle from the polarization data, analyze the phase angle at the same surface point that was identified using the 3D shape obtained by space carving, and compute the surface normal of the whole object surface using the phase angle obtained from multiple viewpoints.

To obtain a detailed representation of the surface shape of the object, we took both the geometrical approach and the photometrical approach. We use the space carving method for the geometrical approach, and the shape-from-polarization method for the photometrical approach. The space carving method can estimate the 3D shape of a textureless object; however, it cannot estimate the detailed smooth structure of the object surface. We therefore use the shape-from-polarization technique to estimate the detailed smooth structure of the object surface. Similar to the space carving method, and unlike the photometric stereo method, the shape-from-polarization method can estimate the surface normal of a highly specular object, even when it is black in color.

III. Experiment

A. Simulation results

First, we estimated the surface normal using the simulation-generated input data. The target object is a smooth sphere, which is assumed to have only specular reflection. The object is illuminated from every direction.

1) Simulation results for a sphere: In our simulation, 12 cameras are set horizontal to the object, and 12 more cameras are set 30 degrees above the object. The arrangement of the simulation is shown in Fig. 6. The angle between each camera is set at 15 degrees. The distance between each camera and the object is the same in this experiment.
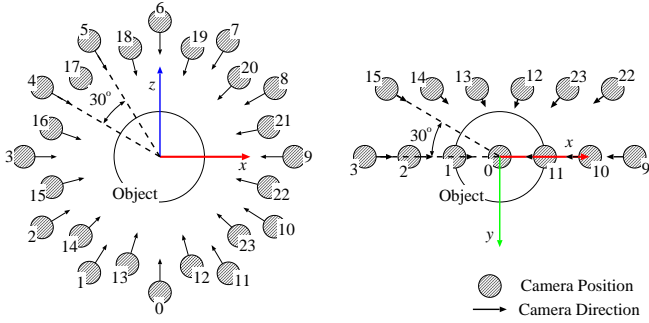
Figure 6. Camera locations for simulation data. (left: vertical view; right: horizontal view)
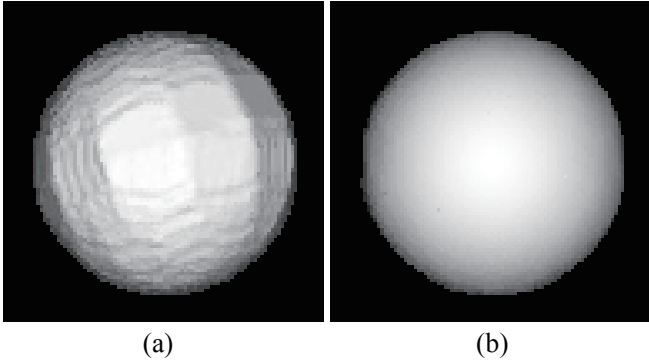

(a)   (b)

Figure 7. (a) Space carving result estimated from simulation data. (b) Our result estimated from simulation data.

The result of the space carving is shown in Fig. 7 (a). The length of the voxel space is 200 [px]. A rough estimate of the shape is obtained using this process. The smooth detailed structure of the surface shape is obtained by introducing the shape-from-polarization technique.

The result for the surface normal obtained through polarization analysis is shown in Fig. 7 (b). The smooth surface of the sphere is clearly estimated. Table I shows the error values for the results shown in Fig. 7. The error is calculated as an angle [rad] between the estimated surface normal and the surface normal of the true shape. Table I shows the average, the maximum, and the minimum of this angle over all surface points. Table I indicates that the error for our result (Fig. 7 (b)) is smaller than that for space carving alone (Fig. 7 (a)).

B. Experiments in real situations

1) Experimental setup: The object is illuminated using a lighting dome, which produces unpolarized light, as shown in Fig. 8 and Fig. 9. The object is set in the middle of the dome, and is rotated using the turntable. The dome is illuminated by a combination of the spotlights, the fluorescent roof lights, and the white wall. We use the PI-100 polarization imaging camera (Photonic Lattice, Inc.), which can measure

Table I
COMPARISON BETWEEN THE ESTIMATED SURFACE NORMAL AND THE TRUE SURFACE NORMAL.

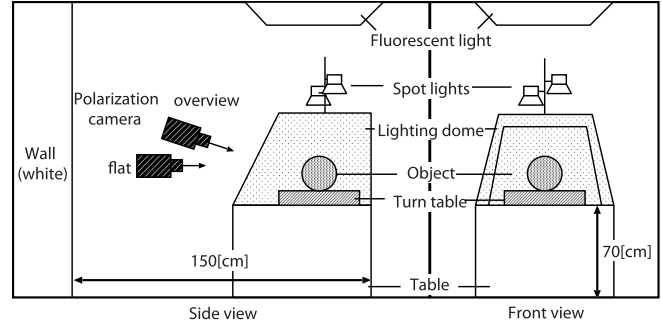|		Space carving result	Our result
Angle between two vectors [rad]	Average	0.100811	0.016366
	Maximum	0.369145	0.121151
	Minimum	0.000000	0.000000

Figure 8. Experimental setup.

the polarization state of the incoming light in real time and in monochrome with 1120×868 [px] resolution.

2) Estimation results for plastic sphere: We use a black plastic sphere as the target object, which has high specularity, as shown in Fig. 10. The diameter of the sphere is 40 [mm]. The results of the space carving are shown in Fig. 11. The length of each side of the voxel space is 400 [px]. Due to the sparse camera arrangement, the space carving cannot represent the smooth surface of the sphere. Our results are shown in Fig. 12. The smooth surface normal of the sphere is estimated clearly using our algorithm. Some estimation errors can be found on the bottom part of the sphere. These errors are caused by the insufficient illumination of the bottom part due to the pedestal for the target object. This result indicates that our method can obtain successful results for smooth black objects.

3) Results for black plastic rabbit: In this section, we estimate the surface normal of a much more complex object, which is shown in Fig. 13. The target object is shaped like a rabbit, which was made by a 3D printer from the 3D polygon data provided by Turk and Levoy [24]. The target object is made from black plastic, which causes high specularity. The object is observed from 24 directions. The phase angle is obtained using the polarization imaging camera.

Fig. 14 represents the true data rendered from the 3D polygon data. The space carving result is shown in Fig. 15. The length of each side of the voxel is 400 [px]. Fig. 15 indicates that space carving methods can only estimate a squarish, non-smooth shape unless a sufficient number of cameras is supplied. The resultant shape estimated using our method is shown in Fig. 16. The smooth curved surface
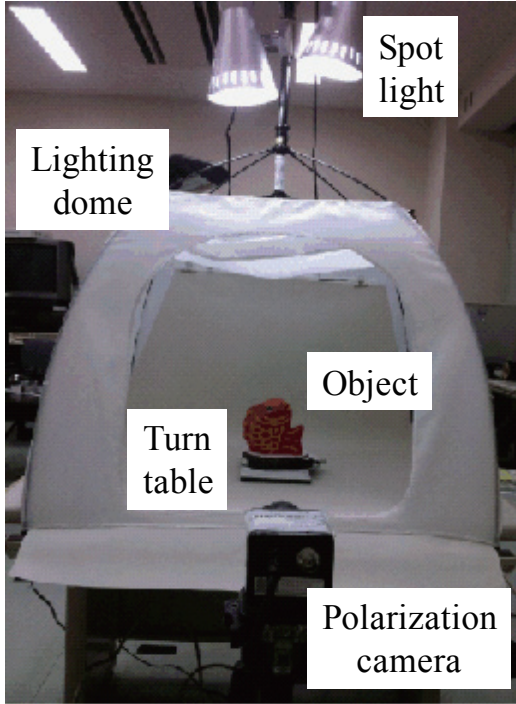
Figure 9. Lighting dome.

Figure 11. Results of space carving for real sphere.
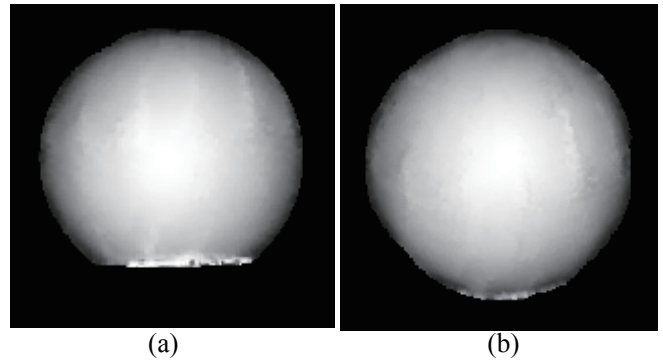
Figure 12. Our results for real sphere

Figure 10. Target plastic sphere.
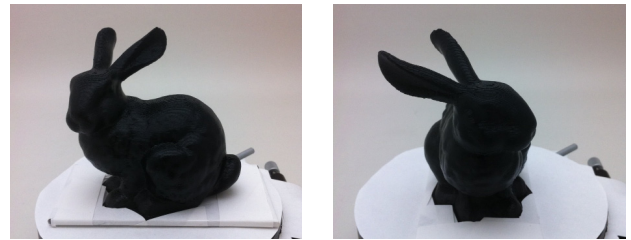
Figure 13.   The real target object Stanford Bunny, generated by a 3D printer.

and the detailed structure of the bulging muscles of the object surface are estimated well. On the other hand, the complex structure of the ear is not recovered clearly. The phase angles of the multiple viewpoints should be analyzed at an identical surface point; however, the corresponding point for the multiple viewpoints is not correctly computed for the space carving results, which show low quality due to the sharp changes in the curvature. In addition to the error at the ear, the foot and the neck of the rabbit were also not well estimated by our method. These parts are not well illuminated because the light is occluded by other parts of the object itself.
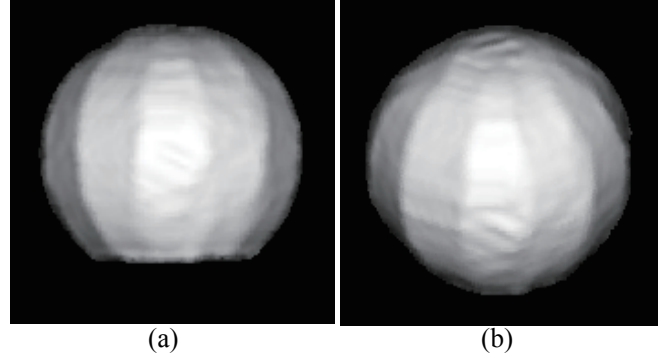
IV. CONCLUSION

We proposed a shape estimation method from polarization images obtained from multiple viewpoints. We have elaborated on the full integration of the advantages of both the space carving method and the shape-from-polarization method. The proposed method computes the surface normal using SVD to minimize the least squares error. The method can estimate the shape of optically smooth objects, such as plastic objects and ceramic objects. The shapes of black objects with high specularity have also been estimated successfully.

The experiments show that our method can estimate the surface normal of optically smooth objects with high
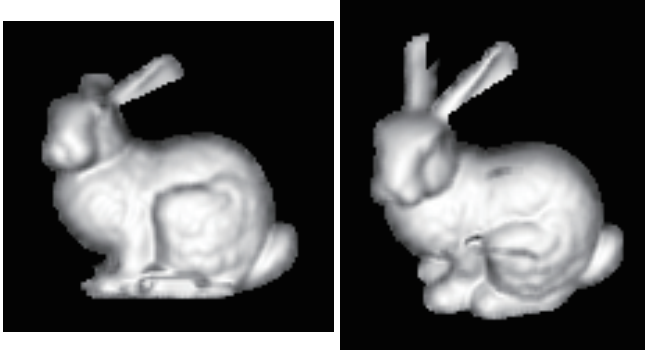
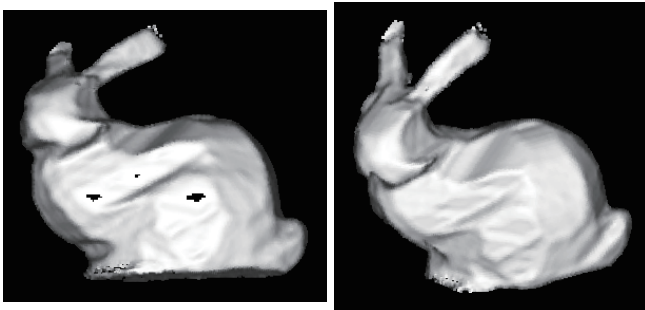Figure 14.   Ground truth of Stanford Bunny.

Figure 15.   Results of space carving for Stanford Bunny.
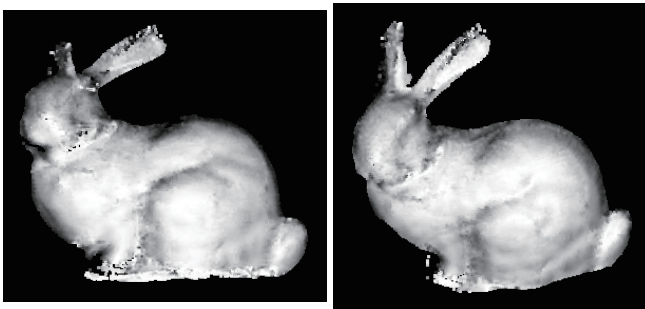

Figure 16.   Our results for Stanford Bunny.

specularity. This property indicates the advantage of the proposed approach when compared with the photometric stereo method, because the conventional photometric stereo method can only estimate the surface normal of diffuse objects.

The final result of our method is a 3D geometrical surface obtained using the space carving method, with the surface normal mapped onto the surface. Although the final rendered image represents a shape similar to the ground truth, the geometrical coordinates of the surface points are still the same as those for the space carving results. However, because the 3D geometrical shape is still far from the true shape, some serious problems may occur in some application fields. Our future work must therefore address the estimation

of the fine details of the 3D geometrical coordinates using the surface normal.

REFERENCES

[1] G. A. Atkinson and E. R. Hancock, "Multi-view surface reconstruction using polarization," in *Proceedings of IEEE International Conference on Computer Vision*, pp. 309–316, 2005. 1

[2] G. A. Atkinson and E. R. Hancock, "Recovery of surface orientation from diffuse polarization," *IEEE Transactions on Image Processing*, vol. 15, no. 6, pp. 1653–1664, 2006. 1

[3] G. A. Atkinson and E. R. Hancock, "Polarization-based surface reconstruction via patch matching," in *Proceedings of IEEE Computer Society Conference on Computer Vision and Pattern Recognition*, pp. 495–503, 2006. 1

[4] M. Born and E. Wolf, *Principles of optics*, Pergamon Press, 1959. 1

[5] P. Fua and Y. G. Leclerc, "Object-centered surface reconstruction: combining multi-image stereo and shading," *International Journal of Computer Vision*, vol. 16, no. 1, pp. 35–56, 1995. 2

[6] E. Hecht, *Optics*, Addison-Wesley, 2002. 1

[7] T. Higo, Y. Matsushita, N. Joshi, and K. Ikeuchi, "A hand-held photometric stereo camera for 3-D modeling", in *Proceedings of IEEE International Conference on Computer Vision*, 2009. 2

[8] K. Koshikawa and Y. Shirai, "A model-based recognition of glossy objects using their polarimetrical properties," *Advanced Robotics*, vol. 2, no. 2, pp. 137–147, 1987. 1

[9] K. N. Kutulakos and S. M. Seitz, "A theory of shape by space carving," *International Journal of Computer Vision*, vol. 38, no. 3, pp. 199–218, 2000. 1

[10] J. Lim, J. Ho, M. H. Yang, and D. Kriegman, "Passive photometric stereo from motion," in *Proceedings of IEEE International Conference on Computer Vision*, pp. 1635–1642, 2005. 2

[11] A. Maki, M. Watanabe, and C. Wiles, "Geotensity: Combining motion and lighting for 3D surface reconstruction," *International Journal of Computer Vision*, vol. 48, no. 2, pp. 75–90, 2002. 2

[12] W. N. Martin and J. K. Aggarwal, "Volumetric descriptions of objects from multiple views," *IEEE Transactions on Pattern Analysis and Machine Intelligence*, vol. 5, no. 2, pp. 150–158, 1983. 1

[13] D. Miyazaki, M. Saito, Y. Sato, and K. Ikeuchi, "Determining surface orientations of transparent objects based on polarization degrees in visible and infrared wavelengths," *Journal of Optical Society of America A*, vol. 19, no. 4, pp. 687–694, 2002. 1

[14] D. Miyazaki, R. T. Tan, K. Hara, and K. Ikeuchi, "Polarization-based inverse rendering from a single view," in *Proceedings of IEEE International Conference on Computer Vision*, pp.982–987, 2003. 1

[15] D. Miyazaki, M. Kagesawa, and K. Ikeuchi, "Transparent surface modeling from a pair of polarization images," *IEEE Transactions on Pattern Analysis and Machine Intelligence*, vol. 26, no. 1, pp. 73–82, 2004. 1

[16] D. Miyazaki and K. Ikeuchi, "Shape estimation of transparent objects by using inverse polarization raytracing," *IEEE Transactions on Pattern Analysis and Machine Intelligence*, vol. 29, no. 11, pp. 2018–2030, 2007. 1

[17] K. Ochiai, N. Tsumura, T. Nakaguchi, K. Miyata, and Y. Miyake, "Gonio-spectral based digital archiving and reproduction system for electronic museum," in *Proceedings of ACM SIGGRAPH 2006 Research posters*, article no. 97, 2006. 2

[18] W. H. Press *et al.*, *Numerical recipes in C: the art of scientific computing*, Cambridge University Press, 1997. 3

[19] S. Rahmann, "Polarization images: a geometric interpretation of shape analysis," in *Proceedings of International Conference on Pattern Recognition*, pp. 542–546, 2000. 1

[20] S. Rahmann and N. Canterakis, "Reconstruction of specular surfaces using polarization imaging," in *Proceedings of IEEE Computer Society Conference on Computer Vision and Pattern Recognition*, pp. 149–155, 2001. 1

[21] S. Rahmann, "Reconstruction of quadrics from two polarization views," in *Proceedings of Iberian Conference on Pattern Recognition and Image Analysis*, pp. 810–820, 2003. 1

[22] M. Saito, Y. Sato, K. Ikeuchi, and H. Kashiwagi, "Measurement of surface orientations of transparent objects by use of polarization in highlight," *Journal of Optical Society of America A*, vol. 16, no. 9, pp. 2286–2293, 1999. 1

[23] W. A. Shurcliff, *Polarized light: production and use*, Harvard University Press, 1962. 1

[24] G. Turk and M. Levoy, "Zippered polygon meshes from range images," in *Proceedings of ACM SIGGRAPH 1994*, pp. 311–318, 1994. 5

[25] L. B. Wolff and T. E. Boult, "Constraining object features using a polarization reflectance model," *IEEE Transactions on Pattern Analysis and Machine Intelligence*, vol. 13, no. 7, pp. 635–657, 1991. 1

[26] R. J. Woodham, "Photometric method for determining surface orientation from multiple images," *Optical Engineering*, vol. 19, no. 1, pp. 139–144, 1980. 2

[27] L. Zhang, B. Curless, A. Hertzmann, and S. M. Seitz, "Shape and motion under varying illumination: Unifying structure from motion, photometric stereo, and multi-view stereo," in *Proceedings of IEEE International Conference on Computer Vision*, pp. 618–625, 2003. 2

[28] T. Zickler, P. N. Belhumeur, and D. J. Kriegman, "Helmholtz stereopsis: Exploiting reciprocity for surface reconstruction," *International Journal of Computer Vision*, pp. 215–227, 2002. 2